Sulfated mannan helps diatoms domesticate their microbiome

J. Krull[1,2,6], C.J. Crawford[4], C. Sidhu[3], V. Solanki[3], M. Bligh[3], L. Rößler[2,3], R.K. Singh[4], G. Huang[2,3], C.S. Robb[2,3], H. Teeling[3], P.H. Seeberger[4], T. Schweder[5,6], J-H. Hehemann[1,2,3]*

[1] BIOM, Faculty of Chemistry & Biology, University of Bremen, Germany

[2] MARUM, University of Bremen

[3] Max Planck Institute for Marine Microbiology, Bremen

[4] Max Planck Institute of Colloids and Interfaces, Potsdam, Germany

[5] Institute of Pharmacy, University of Greifswald, Germany

[6] Institute of Marine Biotechnology, Greifswald

*jhhehemann@marum.de

Significance statement:

Eukaryotes host microbial partners that shape their health, yet how they selectively assemble beneficial microbes remains unclear. Using diatom microalgae as a model, we show they exude a sulfated mannan that nourishes highly adapted bacteria tracking them across the global ocean. Our findings suggest that single-celled eukaryotes can “domesticate” prokaryotes—analogous to how humans have domesticated animals—albeit on a microscopic scale. Dominating much of Earth’s aquatic surface, diatoms drive ~20% of global photosynthesis. We propose that sulfated mannan contributes to this success by helping diatoms shape microbial partnerships that underpin planetary energy balance and atmospheric chemistry.

Abstract

Diatoms are a keystone phylum in Earth's ecosystems, specializing in oxygen production and carbohydrate fixation that fuels global food webs. Diatoms host a microbiome, but how they preferentially collect bacteria with complementary traits remains unknown. Here we show that diatoms exude a C6-sulfated α-1,3-mannan that serves as a selective carbon source for adapted bacteria. Its structure was resolved by NMR spectroscopy, chromatography, chemical synthesis, and enzymatic dissection. Biochemical, physiological, and structural analyses revealed that specialized *Bacteroidota* employ a four-enzyme pathway to metabolize this mannan. Metagenomic and transcriptomic data indicate that the mannan globally selects for bacteria carrying these enzymes and associated traits. Because the mannan provides only carbon, oxygen, sulfur, and hydrogen, bacteria must obtain other essential elements from alternative sources, reinforcing metabolic interdependence. We propose that diatoms use sulfated mannans to attract beneficial partners and exclude competitors, thereby engineering a microbiome that enhances their productivity and underpins carbon cycling.

Main

Domestication (lat. *domesticus,* belonging to the house) is a process where an organism with sufficient access to energy can maintain an environment that hosts other species with complementary traits (1). The process involves reciprocal exchange of molecules and activities enabled through cognate genetic adaptations in the interacting species. Over time, sustained environmental control can lead to the emergence of symbiosis (2) In multicellular eukaryotes, such as animals and plants, slow reproduction rates delay the detection of genetic changes in offspring, making it challenging to detect molecular signatures of domestication (3). As a result, the underlying process of domestication remains largely unknown, especially at the molecular level.

To investigate this process, we considered single celled eukaryotes, diatoms and their associated prokaryotes. In the sunlight fueled surface ocean, diatoms can produce several hundred thousand cells within days in just a milliliter of seawater (1, 4). They photosynthesize organic molecules that sustain the carbon metabolism of associated prokaryotes (4, 5). Importantly, both partners can be cultivated, which facilitates identifying coevolving genes and the molecules that mediate interactions. Some functions resemble feed, fertilizers, herbicides and fences. For example, diatoms release carbohydrates used by bacteria as a carbon source (6, 7). They also release antibiotics (5, 8, 9) that suppress bacteria with incompatible traits, analogous to fences deterring predators or herbicides suppressing weeds. Fed, protected, and relieved of competition, the retained bacteria can concentrate nutrients (10), and return them, along with hormones and vitamins (8, 10, 11), to the auxotrophic algal host. Hence, diatoms and bacteria form a model system to study the process of domestication.

Carbohydrates, such as the abundant carbon energy molecule glucose (100 Gt C annual synthesis rate (18), can mediate both positive and negative interactions. In closed ring form glucose provides energy, but in the open ring form, with an exposed aldehyde group, glucose is toxic. This aldehyde group is one reason why insulin must activate muscle cells to remove excess glucose, as overexposure will cause host cells to die (19). Similar dual effects of

glucose on microbes have been described (20)(21). Thus, the same molecule can serve as both nutrient and toxin, offering hosts a mechanism to reward some partners while excluding others. Such “functional flips” provide a molecular basis for domestication, challenging our positively biased view (22) of how complex communities assemble. Extracting this ancient insight from science, fiction (23), and philosophy (24), and applying it to organic molecules thought to benefit microbes, may help to uncover unknown rules that regulate biomes, including those central to the carbon cycle.

Diatoms exude substantial quantities of organic carbon in the form of complex carbohydrates (glycans) (25-27). These glycans, alongside many other molecules, likely shape the reproducible communities of bacteria attracted to or repulsed by diatoms. These include *Alphaproteobacteria* (e.g., *Candidatus* Pelagibacter ubique; SAR11), *Roseobacteraceae, Gammaproteobacteria (e.g. Vibrionaceae), Bacteroidota (e.g. Polaribacter* spp., *Formosa* spp.), *Cyanobacteria, Verrucomicrobiota,* and many other taxa (28-30). The chemical structures and mechanisms that govern glycan effects on bacteria remain difficult to resolve. A glycan chain with over 1000 monomers, about the length of a bacterial cell, can be highly anionic. Sulfate and carboxyl groups render these glycans extremely surface-active, promoting coagulation with cations, minerals, bacterial cells, proteins, and other molecules (27, 31, 32). The resulting gels impede separation and purification, hindering structural determination. Without defined structures, the ecological effects of glycans on bacteria, with or without the enzymes to metabolize, evade, or extract nutrients, remain obscure.

Here we resolved the structure of a sulfated mannan secreted by diatoms collectively responsible for 20% of global primary production (18). This figure rises to 70% in coastal upwelling zones and ~50% in temperate subpolar regions during spring and summer (33). T The mannan selectively recruits bacteria that harbor a genetic island for mannan utilization, consistently associated with diatoms across the global ocean microbiome. The mannan may mediate association and disassociation between specific bacterial taxa, traits, functions. From a eukaryotic perspective, prokaryotes are rapidly growing, abundant, mobile and accessible

93 sources of essential nutrients. Here we deduce how diatoms may “domesticate” and farm
94 prokaryotes.

95 **Results**

96 **Diatoms may cultivate adapted bacterial taxa by exudation of sulfated mannan**

97 During the analysis of diatom bloom-associated metagenomes and bacterioplankton genomes,
98 we noted the recurrence of bacterial taxa with a putative polysaccharide utilization locus (PUL)
99 for mannan that consistently co-occurred with diatoms (**Fig. 1**). The PUL is found in marine
100 *Bacteroidota* including *Formosa* spp., *Ochrovirga* spp., and *Polaribacter* spp., which are which
101 are globally distributed and often highly abundant, like the diatoms they frequently associate
102 with. Some of these species can account for ~10% of the bacterioplankton cells surrounding
103 diatoms (34-36). We reasoned that, among many organic molecules, a mannan may contribute
104 to a stable microbiome (37-40). To uncover this hypothetical mannan, we worked together with
105 the centric diatom *Conticribra weissflogii* (formerly *Thalassiosira weissflogii*), a diatom model
106 species (41).

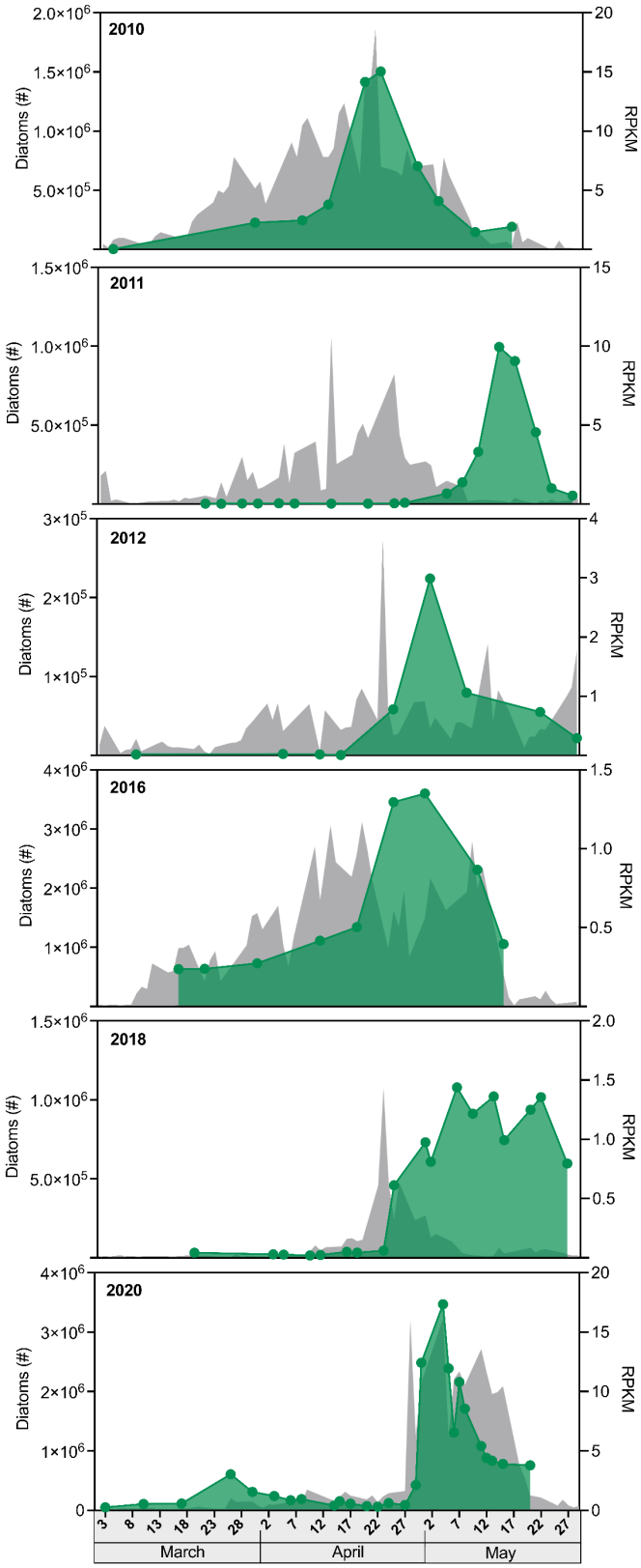

107

108 **Figure 1: *Bacteroidota* with putative mannan utilization enzymes follow diatoms during algal blooms.** Shown

109 are data from six years from the long-term ecological research station (LTER) on Helgoland. The diatoms cells are

110 followed by certain *Bacteroidota* taxa that have a polysaccharide utilization locus (PUL, **Fig. S2**) with putative
111 enzyme and related genes that indicate utilization of a hypothetical, sulfated mannan secreted by the diatoms. The
112 DNA sequence of the mannan PUL of *Polaribacter* sp. Hel1_33_49 was mapped against metagenomes collected
113 previously from the LTER, Helgoland Roads. Grey shows diatom cell counts obtained by microscopy. Green shows
114 the PUL abundance over years calculated in terms of Reads Per Kilobase per Million mapped reads (RPKM). For
115 more information, see Materials and Methods.
116

117 **A C6-sulfated α-1,3-mannan secreted by a diatom**

118 We previously used anionic exchange chromatography (AEX) to show that several diatom
119 species, including *C. weissflogii*, secrete a fucose-containing sulfated polysaccharide (FCSP)
120 of unknown structure (27). By refining AEX chromatography to achieve higher molecular
121 resolution, we found that the material secreted by *C. weissflogii* comprises at least three
122 anionic glycans: the FCSP, a glucuronomannan (42, 43) and a previously unknown
123 homomannan. The FCSP and the glucuronomannan eluted at lower salt concentrations (0.5-
124 1.2 M NaCl) and contained diverse monosaccharides, whereas, the homomannan eluted only
125 at 2 M NaCl **(Fig. S1 A-C)**. Acid hydrolysis coupled with HPAEC-PAD (high-performance anion
126 exchange chromatography with pulsed amperometric detection) revealed a composition of
127 ~95 mol % mannose. Additional ion chromatography revealed that the mannan contains an
128 almost equimolar ratio of sulfate to mannose **(Fig. S1 D)**.

129 During chromatography, concentration, and dialysis, the mannan remained soluble in both
130 seawater and deionized water. It reached solubility up to 20 mg mL^{-1}, the highest tested,
131 whereas other the algal polysaccharides (agar, κ-carrageenan, alginate and pectate) formed
132 gels under seawater concentrations of calcium and magnesium ions (44). These insoluble
133 glycans may target, or be targeted by, distinct bacterial populations (39), in contrast to the
134 soluble mannan. From 160 L of diatom culture, we obtained between 15-20 mg of the mannan
135 (~100 μg L^{-1}).

136

For configuration and connectivity, we used one- and two-dimensional NMR **(Fig. 2 A, B)**. Details are provided in the supplementary information. Briefly, the major component was α-1,3-D-mannopyranose with the C6-carbon de-shielded at 67.5 ppm, consistent with 6-*O*-sulfation and confirming the equimolar mannose-to-sulfate ratio **(Fig. 2B, Supplementary Text)**. For further verification, we synthesized a mannan oligosaccharide and used it as a reference for comparative NMR.

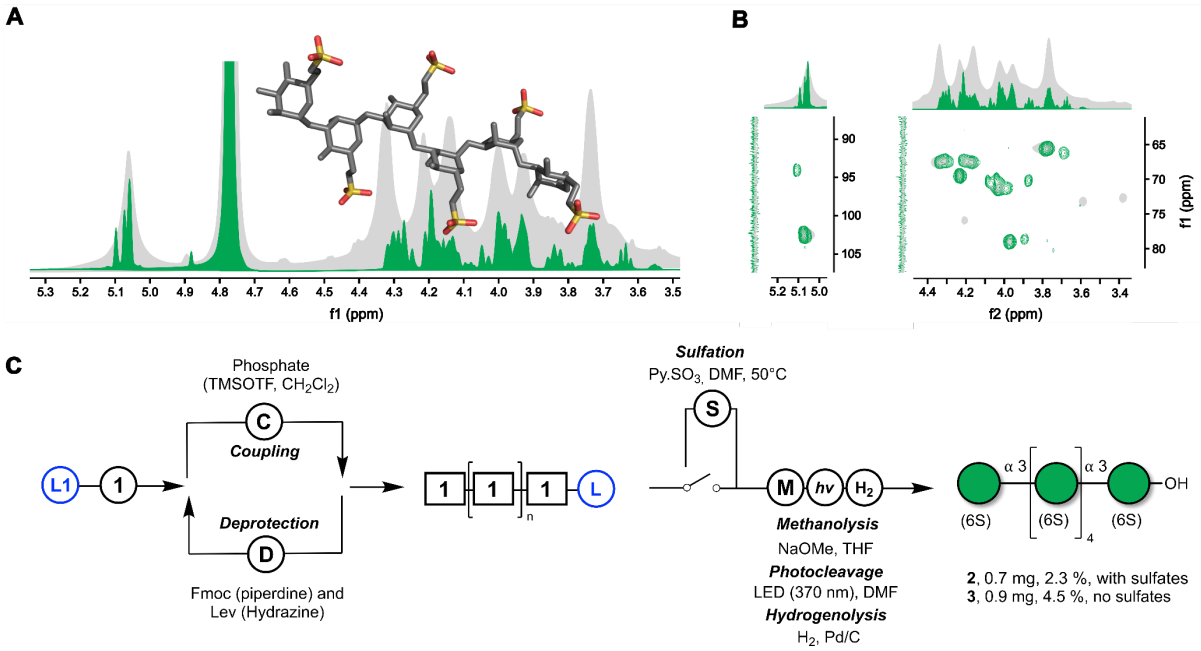

Figure 2: Diatoms synthesize a homomannan made of α-1,3-mannose-6-sulfate. In addition to chromatographic structure elucidation **(Fig. S1 B, D)** we used automated glycan assembly (AGA) to synthesize a mannan oligosaccharide of the NMR-hypothesized structure of the diatom mannan and compared the two spectra. (**A**) ^{1}H-NMR overlay of an automated glycan assembly derived, synthetic α-1,3-mannose-6-sulfate hexaoligosaccharide (green) and the mannan purified from *Conticribra weissflogii* culture supernatant (gray). (**B**) Shown is an overlay of ^{1}H-^{13}C HSQC spectra from the synthetic mannan hexamer (green) and the purified, diatom mannan (gray). NMR spectra at 700 MHz were collected at 20 °C. HSQC-TOCSY and ^{1}H-^{13}C HMBC can be found in supplementary data. (**C**) Scheme of chemical synthesis of mannan oligosaccharides. L1: free reducing end solid-phase linker (45). 1: Dibutyl 2-*O*-benzoyl-4-*O*-benzyl-6-*O*-(9-fluorenylmethoxycarbonyl)-3-*O*-levulinoyl-1-phosphate-α-D-mannopyranoside.

We used automated glycan assembly to synthesize a reference mannan oligosaccharide. As a building block we prepared ethyl-2-*O*-benzoyl-4-*O*-benzyl-6-*O*-(9-fluorenylmethoxycarbonyl)-3-*O*-levulinoyl-1-thio-α-D-mannopyranoside, which was converted

157 into a dibutyl phosphate donor **(1) (Fig. 2C, Supplementary Text).** This enabled the
158 automated assembly of a hexa-α-1,3-mannose bearing one sulfate on each C6. Comparison
159 of NMR spectra from natural and synthetic mannan showed deviations of <0.03 ppm in the
160 proton and <0.1 ppm in the carbon dimension **(Fig. 2 A, B, Table S1)**, confirming the structure
161 as a C6-sulfated α-1,3-mannan. **(Fig. S2)**.

162 ***Polaribacter* spp. can metabolize the mannan**

163 We tested with *Polaribacter* strains - Hel1_33_49, _78 and _96 whether the PUL (46) enables
164 mannan metabolism. These strains have 100% identical 16S RNA genes and 98.5% genome-
165 wide average nucleotide identity (ANI) (47), providing three biological replicates. They have
166 the PUL, indicating a similar ability to metabolize the mannan. Accordingly, when the mannan
167 was provided as a limited carbon source, the three strains grew better **(Fig. S3-6, Table S2)**.
168 As a negative control, we used *Polaribacter* sp. Hel1_88 (36, 46), which lacks the mannan-
169 PUL (37). The Hel1_88 strain grew less on mannan in comparison to Hel1_33_49, _78 and
170 _96. The mannan remained unconsumed in the culture of *Polaribacter* sp. Hel1_88 **(Fig. S4)**.

171 In 2020 we showed *Polaribacter* transcribe this PUL in situ (38), the North Sea. To confirm
172 transcription and translation of enzymes capable of depolymerizing the mannan, we used cell
173 lysates of *Polaribacter* sp. Hel1_33_78 for activity tests. Enzymes were extracted from
174 bacterial cultures grown with or without the mannan **(Fig. S5,6)**. The enzymes in the lysates
175 from cells grown with the mannan digested the mannan. These expression and activity assays
176 suggest these enzymes of adapted *Polaribacter* spp. are for the metabolism of the mannan.
177 The in situ enzyme expression indicates bacteria respond to and interact with the mannan
178 released by diatoms into their environment**.**

179 **The bacterial enzymes can hydrolyze the mannan**

180 To verify enzyme activity and specificity, we used recombinant gene expression, enzymology
181 and structural biology **(Fig. 3)**. The PUL comprises 23 genes **(Fig. S2),** 21 of which encode
182 putative enzymes. We cloned these genes from *Polaribacter* sp. Hel1_33_78 into vectors,
183 transformed and expressed them in *Escherichia coli*, and conducted activity tests using purified

184 mannan, synthesized mannan oligosaccharides, and para-nitrophenyl-labeled substrates
185 (PNP-substrates). The products of these substrates digested with the enzymes were analyzed
186 by fluorophore-assisted carbohydrate gel electrophoresis (FACE) and reducing sugar assays
187 **(Table S3)**. To further substantiate the findings, we obtained homologous enzymes from
188 another marine *Bacteroidota*, *Ochrovirga pacifica* S85, which was isolated from the Pacific
189 Ocean (48) with 69.8% ANI with the *Polaribacter* sp. Hel1_33_78 genome.

190 *O. pacifica* has a distantly related version of the PUL (49) with 68.8% ANI to the mannan PUL
191 of *Polaribacter* sp. Hel1_33_78. We found that the four enzymes are present in both PULs
192 (*Polaribacter*: PbSulf1-GHx, PbGH92_1, PbSulf2; *O. pacifica*: OpSulf1, OpGHx, OpGH92,
193 OpSulf2). These enzymes, comprising one unknown family GHx, one GH92 and two
194 sulfatases, hydrolyzed the mannan into mannose and sulfate **(Fig. 3A)**. The remaining 18
195 putative enzymes were cloned and tested but appeared inactive on the mannan **(Table S3)**.
196 For one sulfatase (OpSulf1) the validity of biochemical experiments could be supported by X-
197 ray crystallography analysis. For the other enzymes, which did not crystallize, we used *in silico*
198 generated AlphaFold2 (50) structure models to falsify the biochemical data.

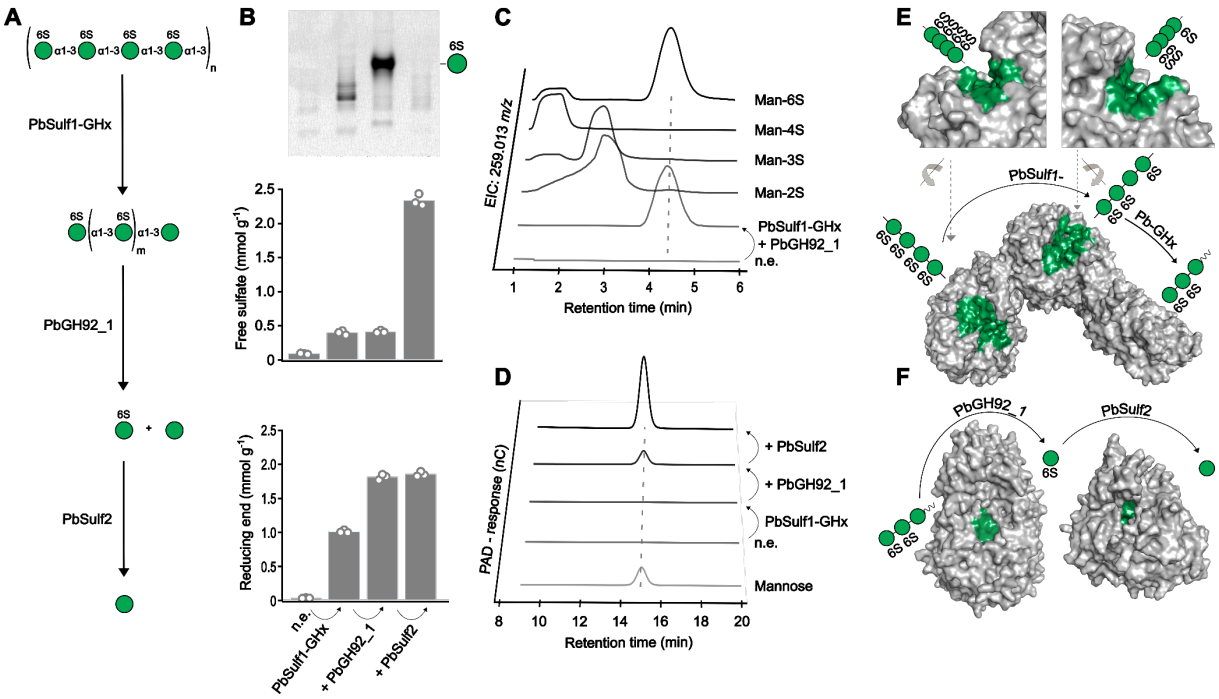

199
200
201 **Figure 3: Four bacterial enzymes in three genes hydrolyze the sulfated α-mannan from diatoms.** (**A**).
202 Suggested degradative pathway for sulfated α-mannan. (**B**) Enzymatic digestions of the mannan via sequentially

203 added PbSulf1-GHx, PbGH92_1 and PbSulf2. Top: Product separation by fluorophore-assisted carbohydrate
204 electrophoresis using 2-aminoacridone as fluorophore. Middle: Free sulfate quantification. Bottom: Reducing end-
205 assay. Bars represent mean of n=3 and circles display individual data points. n.e. = no enzyme. (**C**) Digestion of
206 oligosaccharides produced by PbSulf1-GHx through PbGH92_1 were analyzed using LC-MS. Extracted ion
207 chromatograms at 259.013 *m/z* of the digestion compared with synthesized or commercially purchased mannose-
208 sulfate standards. Man-2S: Mannose-2-Sulfate; Man-3S: Mannose-3-Sulfate; Man-4S: Mannose-4-Sulfate; Man-
209 6S: Mannose-6-Sulfate. (**D**) Mannose release after a sequential digestion of the mannan by PbSulf1-GHx,
210 PbGH92_1 and PbSulf2 detected using HPAEC-PAD. (**E**-**F**) Structural model of enzymes involved in the
211 degradative cascade were generated using AlphaFold2. Active site regions (green color) were identified using
212 structural superimpositions with previously characterized enzymes. A simplified version of the degradative cascade
213 is depicted according to the symbol nomenclature for glycans (51). (**E**) The PbSulf1-GHx tandem enzyme with the
214 rotated active site region of the Sulfatase- and GHx-domain shown in top left and right, respectively. Grey arrows
215 indicate the rotation axis of each domain towards the full-length protein (below). (**F**) Exo-acting PbGH92_1 and
216 PbSulf2 have a pocket shape active site.

217 Mannan degradation is accomplished in four enzymatic steps. The first two steps are
218 completed by the multimodular enzyme PbSulf1-GHx. The enzyme contains a T9SS domain
219 for extracellular secretion. The sulfatase and GHx domain in PbSulf1-GHx work sequentially
220 to catalyze steps one and two of the cascade. The sulfatase domain belongs to the S1 family,
221 subfamily 51 (52). It is the first described activity of this subfamily and the first known sulfatase
222 with this specificity. The GHx domain is distantly related to endo α-1,2 mannanases of the
223 GH99 family and may therefore classify as a new family (53). Separating and visualizing
224 fluorophore-labeled reaction products on FACE gels showed hydrolysis of the mannan by
225 PbSulf1-GHx, producing a ladder-like pattern of oligosaccharides typical for endo-acting
226 enzymes (54) **(Fig. 3B).** The tandem enzyme released sulfate and oligosaccharides as shown
227 by ion chromatography and reducing sugar assays **(Fig. 3B)**. Liquid chromatography mass
228 spectrometry (LC-MS) showed that the released oligosaccharides constituted sulfated hexose
229 oligomers with degrees of polymerization between three and seven **(Fig. S7)**. The
230 oligosaccharides were consistently missing one sulfate group, e.g. a mannose tetrasaccharide
231 had only three sulfate groups, further indicating that both catalytic domains were active on the
232 mannan.

233 We reproduced the results with enzymes from *O. pacifica,* which encodes the two catalytic
234 domains as two separate genes. The enzymes OpSulf1 and OpGHx exhibit 53% and 36%
235 amino acid identity to the respective PbSulf1-GHx domains. The separated enzymes showed
236 that prior sulfatase activity is indeed necessary for GHx activity, suggesting that this enzyme
237 requires a desulfated mannose for productive binding **(Fig. S8)**. The AlphaFold2 model of
238 PbSulf1-GHx showed two appended catalytic domains with open, extended clefts **(Fig. 3E)**
239 typical for endo-acting glycoside hydrolases (54) and sulfatases (55), corroborating the
240 biochemical experiments. We obtained diffraction data from a crystal structure for the OpSulf1
241 at 1.49 Å resolution (**Fig. S9, Table S4**). The crystal structure confirmed an extended substrate
242 binding cleft compatible with the elongated mannan chain. The conserved catalytic residues
243 present in the center may remove one sulfate from the center of the bound mannan chain,
244 which then becomes accessible to the GHx **(Fig. S9B, C)**. In conclusion, we identified and
245 characterized two new enzyme activities, one endo C6-sulfate α-1,3-mannanase forming a
246 new CAZy family, and an endo C6-sulfate α-1,3-mannan sulfatase. These predicted outer
247 membrane enzymes may produce oligosaccharides of suitable size and shape for import into
248 the periplasm.

249 The third step in the mannan degradation cascade was catalyzed by the periplasmic
250 PbGH92_1, a mannosidase that removed C6-sulfated mannose from the oligosaccharides.
251 Periplasmic localization of PbGH92_1, which belongs to the GH92 family (56), was predicted
252 by the Sec/SPI signal peptide (57). The GH92 family includes Ca^{2+}-dependent exo-acting α-
253 1,2/3/4/6 mannosidases, but an enzyme acting on, specific for sulfated mannan remains
254 unknown. Hydrolysis of oligosaccharides into mannose-6-sulfate and a minor amount of
255 mannose was shown by FACE, reducing sugar assays and HPAEC-PAD **(Fig. 3B-D)**. The
256 mannose-6-sulfate product was verified using LC-MS **(Fig. 3C)**. For this analysis, we
257 synthesized mannose-2/3/4-sulfate isomers **(Supplementary Text, Data S1, Fig. S10)**. The
258 retention times revealed that only the mannose-6-sulfate aligned with the enzyme product peak
259 and therefore confirmed this isomer as the product of the PbGH92_1 **(Fig. S11)**. The
260 AlphaFold2 model showed a pocket topology of size and shape typical for an exo-acting GH

261 **(Fig. 3F)** binding one monomer in the -1 subsite (54). Conclusively, PbGH92_1 is a 6-sulfate
262 α-1,3-mannosidase, representing a new specificity within the GH92 family.

263 The fourth step was catalyzed by PbSulf2 that desulfates mannose-6-sulfate to yield mannose.
264 A periplasmatic location was predicted by a Sec/SPII signal peptide. PbSulf2 is classified into
265 sulfatase family S1, subfamily 11. Enzymes in this subfamily have been described to act on
266 glucosamine-6-sulfate (58) and 6-sulfated porphyran oligosaccharides (59), but not on
267 mannose-6-sulfate. PbSulf2 removes a sulfate group from mannose-6-sulfate as shown by
268 appearance of the final product mannose in HPAEC-PAD measurements **(Fig. 3D)** and the
269 disappearance of sulfated mannose in a complementary FACE experiment **(Fig. 3B).** The
270 AlphaFold2 model aligned with the two previously described subfamily members (PDB ID
271 Codes 5G2V / 7LJ2, rmsd: 0.613 Å / 0.845 Å) and showed a pocket topology typical for exo-
272 acting sulfatases (55). PbSulf2 is a mannose-6-sulfate sulfatase, representing a new
273 specificity within this enzyme family.

274 In summary, we elucidated a minimal enzymatic cascade consisting of four enzymes that
275 achieve complete hydrolysis of the mannan into mannose and sulfate. The oligo- and
276 monosaccharide structures produced by the enzymes confirmed the mannan structure solved
277 with NMR.

278 **Biocatalytic quantification of mannan synthesis and degradation**

279 To verify and quantify the synthesis of the mannan by diatom cells and its consumption by
280 adapted *Polaribacter* spp. we used the here characterized enzymes to develop a quantitative
281 assay. The assay involved a combination of chromatography and enzyme digest steps for
282 structure-specific quantification. The enzymes specifically produce mannose that provides a
283 much stronger signal than the undigested polysaccharide with different quantitative
284 approaches, e.g., reducing sugar assay or HPAEC-PAD **(Fig. S12A)**. Chromatographic
285 separation and enrichment of the mannan were crucial for enzyme digestion. Without this
286 purification step, we found the enzymes remained inactive, potentially due to sulfate groups
287 from FCSP or other sulfated glycans binding to and interfering with the enzymes in the mixture

288 (60). After chromatographic isolation of the mannan, the biocatalytic assay detected up to
289 842 ± 62 µg L^{-1} in the diatom culture supernatant **(Fig. 4A).** The concentration was positively
290 correlated with the number of diatom cells ($y = 3.97 \times 10^{-3}\ x - 2.94 \times 10^{-2}$, $P = 1 \times 10^{-23}$, R^2 =
291 0.95). Each individual *C. weissflogii* cell produced on average a net amount of 3.9 fmol carbon
292 in form of mannan **(Fig. 4B).** Substantially less mannan was present in diatom cells or particles
293 **(Fig. S12B,C).** Notably, this new biocatalytic assay detects almost ten-fold higher
294 concentrations (842 ± 62 µg L^{-1}) compared to our initial assessment (~100 µg L^{-1}) based on
295 the preparative mannan purification yield, highlighting the analytic value of enzyme-based
296 assays.

297 Next, we conducted growth experiments with *Polaribacter* sp. Hel1_33_49 and applied the
298 biocatalytic assay to quantify mannan consumption **(Fig. 4C)**. The bacteria grew to an OD_{600}
299 of 0.2 when providing 0.1% (w/v) of the mannan as the limiting carbon source. Mannan
300 concentration and bacterial abundance were negatively correlated ($y = -5.62\ x + 1.09$, $P = 1 \times$
301 10^{-18}, R^2 = 0.96) **(Fig. 4D)**. Conclusively, under nutrient-replete conditions, the bacteria can
302 remove the mannan within a few days.

303 To test whether other diatoms also release this type of mannan, we adapted the biocatalytic
304 assay into a qualitative version that rapidly identifies the structure in different species. We
305 tested *Thalassiosira pseudonana*, *Thalassiosira rotula* and *Chaetoceros affinis,* genera of
306 global ecological and biogeochemical relevance (34). We used AEX to enrich the mannan from
307 each culture supernatant, applied the enzymes and analyzed the products using FACE **(Fig.**
308 **4E, F)**. For each diatom the first two enzymes (PbSulf1-GHx) produced the same set of
309 oligosaccharides that we identified above as oligomers of C6-sulfated α-1,3-mannose missing
310 one sulfate group. PbGH92_1 released mannose-6-sulfate, showing that the same mannan
311 structure is produced by different diatoms common around the globe.

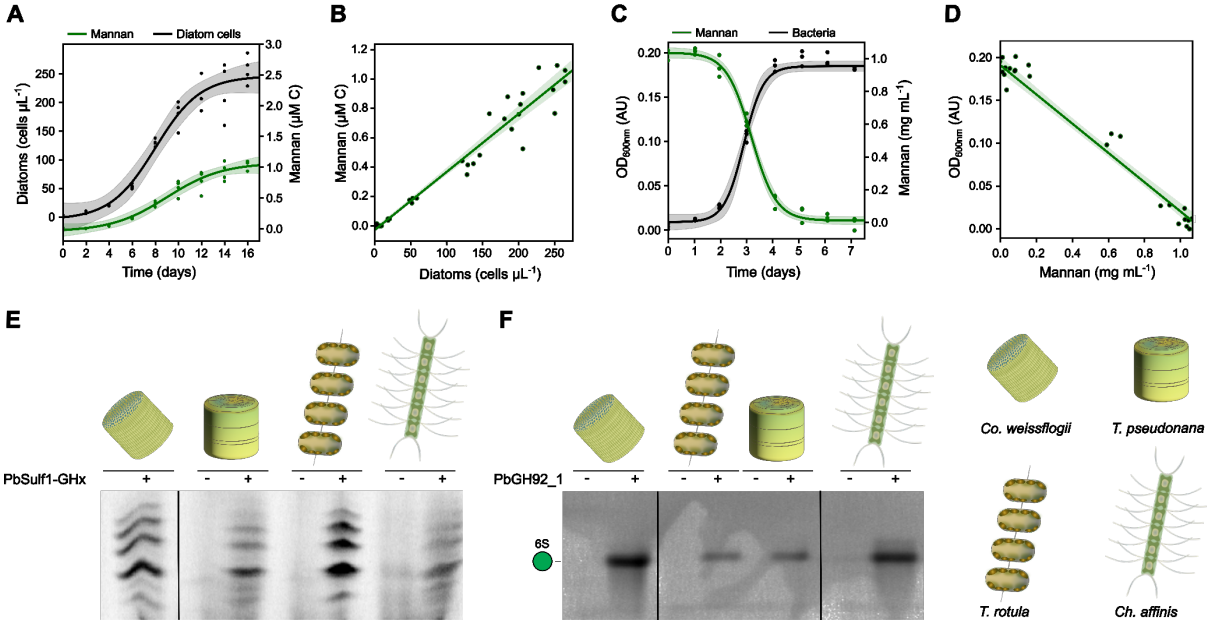

Figure 4: Synthesis of mannan by diatoms and consumption by bacteria quantified with the mannan degrading enzymes. (**A**). Growth analysis of *Conticribra weissflogii* cultures using cell counts (black) and enzymatic quantification of sulfated α-mannan (green) in the anionic fraction of the culture supernatant. Data points were modeled using a logistic growth function employing the non-linear least squares method for fitting. n=4. (**B**) Linear regression analysis of diatom cell counts vs. mannan C production. The net production of mannan per cell was 3.9 fmol C cell^{-1} with an R^2=0.95. (**C**) *Polaribacter* sp. Hel1_33_49 grown with purified mannan for one week at 18 °C. The black line represents optical density measured at 600 nm. The green line shows the mannan consumption as detected via enzymatic quantification. Data points were modeled using a logistic growth function employing the non-linear least squares method for fitting. n=3. (**D**) Linear regression analysis of mannan concentration vs. optical density of the growth curve. (**E-F**) Mannan identification in anionic exudates purified from 0.5-5 M NaCl from AEX from *Conticribra weissflogii*, *Thalassiosira pseudonana*, *Thalassiosira rotula* and *Chaetoceros affinis*. Products were digested with PbSulf1-GHx (**E**) and PbGH92_1 (**F**) and analyzed via fluorophore-assisted carbohydrate electrophoresis using 8-aminonaphthalene-1,3,6-trisulfonic acid (**E**) or 2-aminoacridone (**F**) as fluorophore. Negative controls (-) contained heat inactivated enzyme.

Mannan draws adapted bacteria towards diatoms around the globe

To test the hypothesis that the mannan selects for bacteria with these enzymes we quantified the mannan PUL within the *Tara* Oceans metaG dataset (61). As negative and positive controls for glycan structure-based selection of adapted microbiome members, we used bacterial PULs specific for known glycans from red, green and brown algal phyla. Preconditions for the PULs used as controls were that their target glycans are soluble and therefore accessible to

333 planktonic bacteria, that the glycan structure has been verified by NMR and/or other methods,
334 and that the structure and function of the PUL or of a closely related variant has been
335 empirically verified with biochemical experiments. As negative control we used porphyran, a
336 mixed linked α-, β-galactan that is also sulfated on C6, and the corresponding PUL from the
337 flavobacterium *Zobellia galactanivorans* Dsij^T (62, 63). Compared to diatoms, porphyran-
338 producing red macroalgae *Porphyra* spp., are sessile, require rocks or other hard substrates,
339 grow along coasts. This range restriction makes the corresponding porphyran-PUL a suitable
340 negative control.

341 As a positive control, we used laminarin (chrysolaminarin), a β-glucan that is also produced by
342 diatoms, and the corresponding PUL from a metagenome-assembled genome (MAG
343 C_MB344, accession: GCA_943788335) of a flavobacterial *Aurantivirga* species (38, 64, 65).
344 Finally, we used ulvan, a sulfated rhamnogalacturonan produced by green macroalgal species
345 including *Ulva* spp. *Ulva* spp. grows attached and planktonic, moves via currents between
346 coastal and offshore regions (66), hence whether they, corresponding PUL can serve as
347 negative or positive control was unclear. The corresponding PUL (67) is from the
348 flavobacterium *Formosa agariphila* KMM 3901^T (68, 69).

349 Mannan PUL abundances ranged from 0.0025 to 0.41 RPKM in the 45 sampled sites including
350 open and coastal ocean areas of the Atlantic, Pacific and Indian Ocean (**Fig. S13A**). Higher
351 mannan PUL abundances were detected at upwelling sites (Benguela: 0.41 RPKM, Chile: 0.06
352 RPKM, Peru: 0.03 RPKM, California: 0.04 RPKM) where higher nutrient concentrations
353 enhance diatom-dominated algal blooms (70, 71). The positive control, laminarin PUL showed
354 comparable abundances between 0.006 and 2.27 RPKM **(Fig. S13C)**. The porphyran PUL
355 showed the lowest RPKM values of the tested glycans and was absent in the open ocean **(Fig.
356 S13E)**, as expected for this negative control. The ulvan PUL showed abundances between
357 0.002 and 0.08 RPKM but at different locations compared to the mannan and laminarin PULs
358 **(Fig. S13D)**. The observed differences between the compared groups were significant across
359 the dataset (Friedmann-Test: $P = 6 \times 10^{-21}$).

360 Metagenomics of bacterioplankton and eukaryotic 18S rRNA-based taxonomy revealed that
361 the mannan PUL is associated with diatoms. To verify that diatoms were the main
362 phytoplankton associated with the large RPKM values of PULs at the time of sampling for the
363 *Tara* Ocean metaG dataset, we used previously reported total V9 read numbers as a proxy for
364 diatoms and correlated those with PUL reads (71). This approach was previously verified by
365 showing that V9 reads correlate with diatom algal cell counts (72). At the sites where
366 microalgae were measured, diatoms were a major phytoplankton group (71). Linear regression
367 analyses showed that the abundance of the mannan PUL correlated with diatom read numbers
368 ($y = 7.7 \times 10^{-5}\ x + 6.2 \times 10^{-3}$, $P = 1.5 \times 10^{-3}$, $R^2 = 0.44$) **(Fig. 5A)**. The laminarin PUL also
369 significantly correlated with diatom abundance ($y = 7.3 \times 10^{-4}\ x + 1.7 \times 10^{-3}$, $P = 6.0 \times 10^{-4}$, R^2
370 $= 0.49$) **(Fig. 5B)**. In contrast, we did not observe correlation between the ulvan PUL and
371 diatom cell abundances ($P = 0.35$; $R^2 = 0.05$), which is consistent with the synthesis of this
372 glycan by green algae instead of diatoms **(Fig. C)**.

373 Diatoms are the only known microalgae that synthesize both, the mannan and the laminarin.
374 Hence, we asked whether the PULs for those two glycans co-occurred, which would further
375 support that diatoms are the source of these carbon-rich structures. We found a strong linear
376 relationship between mannan and laminarin PULs ($y = 0.158\ x + 5.35 \times 10^{-3}$, $P = 4 \times 10^{-24}$, $R^2 =$
377 0.91, **Fig. 5F**). In contrast, the PULs for mannan and ulvan did not correlate ($P = 0.414$; $R^2 =$
378 0.02). Finally, we queried for gene expression of the Polaribacter GH92 and found transcripts
379 in the *Tara* Ocean metaT dataset (61). The presence of transcripts suggests associated
380 bacteria degrade the mannan released by diatoms globally (**Fig. 5E)**. Spatially, temporally and
381 phylogenetically separated micro- and macroalgae produce distinguished glycans.
382 Conclusively, these diatom glycans, which select for specifically adapted bacteria, may
383 contribute to the formation of a functional and predictable mosaic of host specific microbiomes
384 in the sunlit ocean.

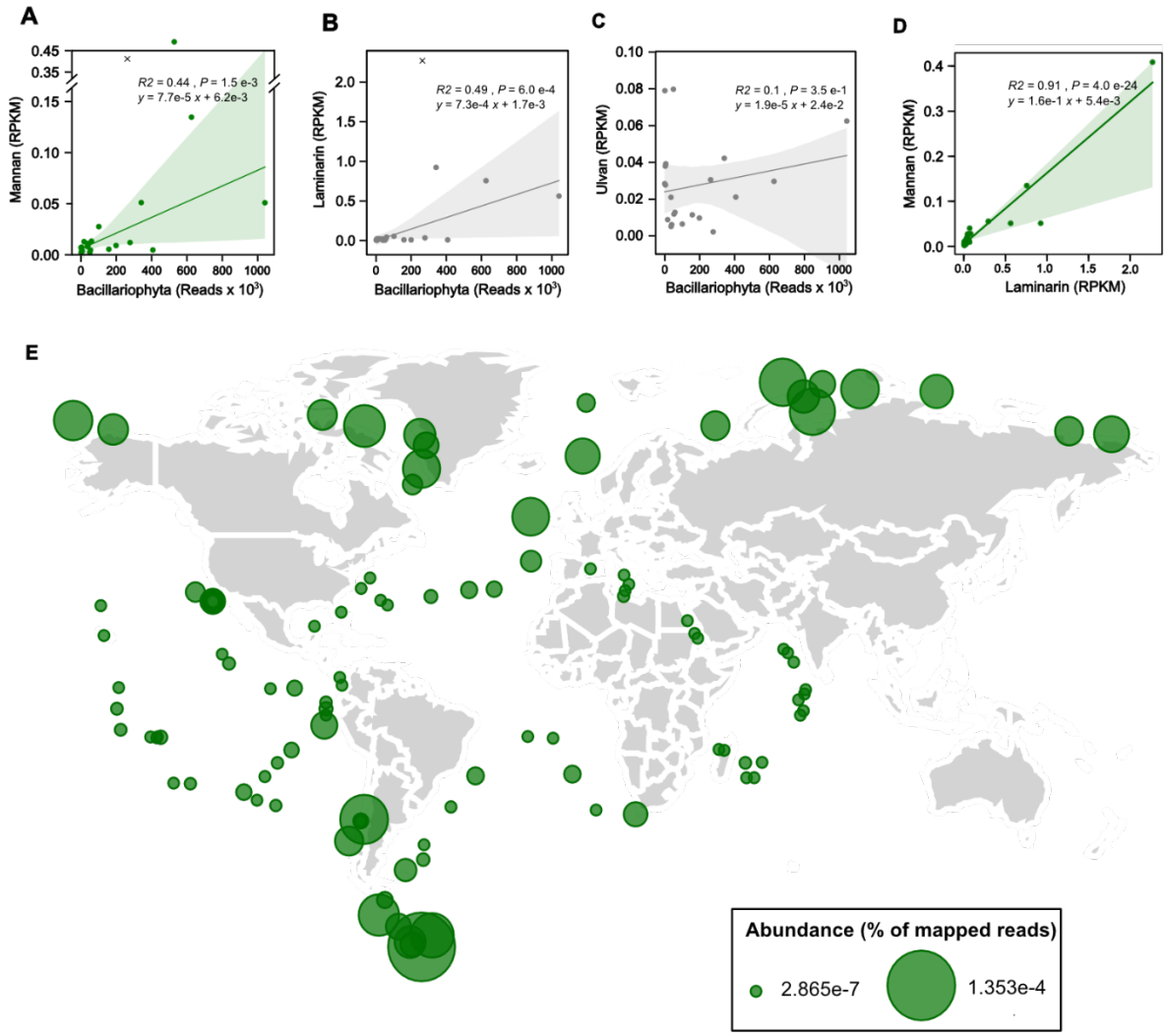

Figure 5: Bacteria with mannan degrading enzymes follow diatoms around the globe. Global abundance of the mannan utilization locus from *Polaribacter* sp. Hel1_33_49 from *Tara* Oceans database. The DNA sequence of the Mannan PUL was mapped against the raw metagenome reads of *Tara* Oceans surface water samples filtered at sizes ranging 0.2-3 µm across 45 different stations (61). Read abundances were calculated in terms of RPKM and normalized by length of the PUL and displayed as filled circles in SI. Corresponding plots for the laminarin PUL from *Aurantivirga* MAG C_MB344 (38), the ulvan PUL from *Formosa agariphila* KMM 3901^T (67) and the porphyran PUL from *Zobellia galactanivorans* Dsij^T (62) can be found in SI. (**A**) Raw read abundance of the clade of Bacillariophyta within the V9 rDNA metabarcoding dataset from *Tara* Oceans surface water samples filtered at sizes ranging 5-20 µm across 35 stations. Please note: No diatom data were available for the remaining stations. (**B-D**) Linear regression analyses of raw read abundance of Bacillariophyta in V9 rDNA metabarcoding dataset from *Tara* Oceans versus RPKM of different PULs across the same stations. Outliers where identified individually for each plot using the studentized residuals method with a threshold of three and excluded from the linear regression. Plots display the correlation analysis of Bacillariophyta vs. (**A**) mannan PUL, (**B**) laminarin PUL and (**C**) ulvan PUL. (**D**) Linear regression analyses of mannan PUL and Laminarin PUL RPKM within the *TARA* Oceans metagenomes. **(E)**

400 The GH92 sequence from the *Polaribacter* cascade was searched against the Tara Oceans OM-RGCv2 database,
401 which includes meta-transcriptomic (metaT) data, using BLASTp with an E-value cutoff of ≤ 1e-20 through the
402 Ocean Gene Atlas v2 web platform. The resulting hits were used to calculate relative abundance, expressed as the
403 percentage of mapped reads.
404

405 **Discussion**

406 Here we show that diatoms secrete a system of anionic glycans that shape microbiomes in
407 multiple ways. The structurally complex FCSP may protect against enzymatic degradation and
408 invasion (73). The carboxyl groups of glucuronomannan may chelate rare trace metals (74).
409 In contrast, the structurally simple mannan provides an easily accessible carbon source for
410 adapted bacteria such as *Polaribacter* spp. which in return supply diatoms with missing
411 nutrients, metabolites and vitamins (75). The characterized enzyme cascade can now be
412 applied to quantify this mannan and assess its role in the carbon cycle (76). The global
413 abundance of mannan degrading enzymes **(Fig. 5)** underscores its ecological importance.

414 The mannan can influence microbes both positively and negatively because sulfation renders
415 glycans protein surface-active. Negatively charged sulfate groups bind to positively charged
416 amino groups of proteins, and potentially interfere with their function (60). C6-sulfation extends
417 the sulfate group farther from the sugar backbone, allowing it to reach positively charged
418 residues even in protein pockets (62). Indeed, cation exchange resins designed to bind
419 diverse protein surfaces with high capacity often use sulfated polysaccharides (77). C6-
420 sulfation may be one of the reasons explaining why, of the three anionic diatom glycans, the
421 mannan was the strongest binder of the surface-exposed amines **(Fig. S1 A-C).**

422 Prokaryotes depend on proteins to degrade, sense, bind, infect, import, move, replicate,
423 transfer, and communicate (78). Many protein structures contain surface-exposed arginine,
424 lysine or histidine residues that can be targeted by sulfate groups (77). This hypothesis aligns
425 with Wheeler and colleagues who uncovered that mucilage glycans exuded by animal epithelia
426 "tame" bacteria by binding to virulence proteins (79). By analogy, diatom-derived mannans
427 may bind proteins across bacteria, eukaryotes, or even viruses, reducing their invasive
428 potential.

429 During algal blooms, sulfated glycans secreted by diatoms, including the mannan **(Fig. S1 A-**
430 **C)**, coagulate into aggregates that entrap bacterial cells, proteins, minerals and other
431 molecules (27, 80-82). Bacteria can bind those glycans, or be bound by them. This interaction

432 may especially capture cells lacking evasive mechanisms, promoting their incorporation into
433 sinking particles. The outcome is a relative increase of some taxa and a decline of other in the
434 sunlit ocean. As dominant algal taxa shift, their exuded sulfated glycans also change, selecting
435 for new bacterial traits **(Fig. 5)** and driving host-specific microbiomes (83, 84).

436 Trade-offs may shape adaptive strategies used by bacteria to evade surface-active glycans.
437 By digesting the mannan the *Polaribacter* spp. "domesticated" by diatoms obtain both carbon
438 and energy, while also removing the interference caused by sulfation. In contrast, bacteria,
439 lacking these enzymes minimize interaction as an alternative defense strategy. For instance
440 SAR11 *Alphaproteobacteria*, among the most successful groups of bacterioplankters around
441 diatoms (85), have a "non-stick" cell surface that bind fewer surface-active glycans (86). This
442 reduced binding is thought to underlie their greater resistance to grazing (86), but it comes at
443 the cost of being unable to access glycan-derived carbon. Similar trade-offs are seen in
444 Roseobacteraceae (75), which focus on smaller organic molecules as carbon sources (87). By
445 avoiding competition for glycans, they maintain a free-living, planktonic lifestyle that
446 nonetheless supports a "domesticated" association with diatoms.

447 This "competition-dispersal" tradeoff has been described in *Vibrio cyclitrophicus,* where closely
448 related strains show signs of recent sympatric speciation into two groups: strong vs. weak
449 binders (88). Strains with surface pili, including the mannose sensitive hemagglutinin (MSH)
450 type involved in host infection (89), bind and exploit surface glycans more effectively than the
451 strains lacking MSH genes. However, non-piliated strains, though less efficient at glycan
452 binding and exploitation, can avoid being irreversibly trapped by glycans (90). Surface-active,
453 adhesive glycans (27) may therefore disproportionately bind bacteria that rely on MSH pili or
454 other attachment proteins, constraining those most poised to intimately interact with eukaryotic
455 hosts. Similar mechanisms operate in animals: epithelial cells secrete the heavily glycosylated
456 immunoglobulin A (IgA) to constrain pathogens. IgA enchains and immobilizes bacteria in
457 aggregates, facilitating their clearance from the intestine (91). Cells trapped by glycans or
458 glycoproteins can be expelled or separated from microbiomes by multiple processes, including
459 bowel movements (91), sinking (83), filtration (27) and consumption (86).

460 In summary, glycans can simultaneously support (92, 93) and suppress (79, 94) bacterial traits.
461 Highly defensive types such as SAR11, with cell surfaces that minimize interaction, or
462 *Polaribacter* spp., equipped with enzymes to deconstruct glycans, can avoid being trapped. In
463 contrast, offensive bacteria such as Vibrio, rich in surface exposed proteins for attachment,
464 degradation, or infection, are more easily trapped and may therefore remain rare (95, 96).
465 Alternatively, they may be "tamed" by glycans, downregulating interactive surface proteins,
466 while upregulating dispersal proteins such as flagella (79). This short-term adaptation, imposed
467 by surface-active glycans, enhances dispersal, reduces competition (90), and protects the host
468 with its domesticated partners. While we highlighted only a few cases, such interactions likely
469 affect every cell to some extent. Through this dual capacity to nourish and constrain, glycans
470 contribute to the emergence of beneficial microbiomes and productive hosts.

471 To conclude, with sufficient light, CO_2, and nutrients, bacteria cannot escape the abundance
472 of photosynthesis-derived surface-active glycans. Around diatoms, these glycans enforce a
473 "domesticated" state through long-term genetic adaptation, or a non-virulent, tamed phase
474 through short-term physiological shifts. Improved molecular understanding will help resolve
475 uncertainties in the large-scale application of such glycans. Future work should focus on the
476 mechanisms by which surface-active glycans protect the collective of domesticated
477 prokaryotes and their eukaryotic hosts against competition, predation, and infection.

478 This process of "domestication" is important in today's context. By fixing CO_2 into simple
479 glycans, diatoms sustain rapidly growing bacteria that in turn boost diatom productivity. In
480 response, diatoms invest in more complex glycans that resist degradation, locking away
481 carbon. Through these reciprocal interactions, mutualistic and antagonistic alike, CO_2 is fixed
482 into glycans in ways that reinforce climate stability. Thus, by secreting sulfated glycans that
483 both nourish and constrain, diatoms domesticate their microbiomes, a microscopic strategy
484 with planetary consequences.

485

Materials and Methods

Mannan PUL abundance in *TARA* Oceans dataset

Metagenome data of bacterioplankton during spring phytoplankton blooms was generated in previous studies (29, 38-40, 97). For the global analysis, we used metagenome data from the *TARA* Oceans Expedition (61). The surface water metagenomes (0.2 to 3 µm) from 45 different stations were included in the analysis. Mapping of PULs was done with Bowtie2 (98) in the SqueezeMeta v1.6.2 pipeline. PUL abundances as reads per kilobase per million mapped reads (RPKM) were calculated using the formula: (metagenome reads mapped to the PUL*10^6)/(length of PUL in kbp × total reads in a metagenome). For correlation of PULs to diatom abundance, we extracted the read numbers from 25 surface water samples (5-20 µm) from the eukaryotic V9 metabarcoding data (71).

Mannan purification

C. weissflogii was cultured non-axenic in NEPCC medium (99). Diatom growth was monitored by cell counting using a Neubauer counting chamber (Marienfeld, Königshofen, Germany). Cells were separated from culture the supernatant using a continuous flow centrifuge (Thermo Fisher Scientific, Walthan, MA, USA) set at 150 mL min^{-1} and 6800 x g. The culture supernatant was filtered using a peristaltic pump through Whatman® glass microfiber filters (Grade GF/F, 0.70 µm). 160 L of *C. weissflogii*, cell and debris free, culture supernatant were loaded onto a preparative scale, self-assembled AEX column. Elution occurred with appropriate NaCl concentrations. Samples were dialyzed against MilliQ water (Merck) and freeze-dried prior to monosaccharide composition and sulfate analysis.

Monosaccharide composition and sulfate content analyses

Purified mannan was dissolved in MilliQ water at 1 mg mL^{-1} and hydrolyzed by 1 M HCl (100 °C, 24 h) in in pre-combusted glass vials. HCl was removed by vacuum or diluted 1:1000 in MilliQ water (Merck) prior to further analyses. Monosaccharide measurements occurred as described previously using a Dionex ICS-5000+ system (Thermo Fisher Scientific) (100) and

512 for sulfate measurements we used a Metrohm 761 compact ion chromatograph (Metrohm,
513 Herisau, Switzerland). All samples for monosaccharide and sulfate composition were prepared
514 in triplicates.

515 **Cloning of enzyme genes into plasmids, recombinant expression and purification**

516 Genes were cloned using the USER cloning or Gibson assembly methodologies (New England
517 Biolabs, Ipswich, NE, USA) with genomic DNA from *Polaribacter* sp. Hel1_33_78. Primer pairs
518 are provided in supplementary table S2. USER cloning constructs were cloned into the pet28A
519 vector (101) without signal peptides (102). Clones were validated by DNA sequencing.
520 Plasmids transformed into *E. coli* BL21 (DE3) were induced in 1 L lysogeny broth (LB) medium
521 containing kanamycin and isopropyl-β-D-1-thiogalactopyranoside (IPTG). For sulfatase
522 activation, the formylglycine generating enzyme plasmid (Addgene plasmid repository,
523 Watertown, MA, USA) (103), which was co-transformed, was induced with L-arabinose and
524 ampicillin added right before cooling to 12 °C. Protein purification was conducted using
525 standard procedures (104).

526 **Enzyme activity and specificity assessment**

527 Enzyme reactions were carried out in 10 mM MOPS pH 7.5 and 500 mM NaCl with 0.1% (w/v)
528 of mannan and enzymes were added in excess (0.01-0.1 mg mL^{-1}). 3.5% Sea Salts (Sigma
529 Aldrich, Burlington, MA, USA) were also added. Enzyme reactions were monitored using
530 fluorophore-assisted carbohydrate electrophoresis (FACE) with carbohydrates labeled with 2-
531 aminoacridone as described in (105). Reducing-end measurements were carried out using
532 PAHBAH as detection reagent as described previously (7). The release of sulfate and
533 mannose from enzymatic reactions were measured using ion chromatography and HPAEC-
534 PAD. Enzymatic assays were carried out as technical replicates in triplicates unless otherwise
535 stated.

536 **Crystallization, data collection, structure solution, refinement and AlphaFold2**

537 Crystallization was performed in two drop 96-well crystallization plates in sitting drop format
538 using commercial crystallization screens. Diffraction data was collected on DESY beamline
539 P11. Measured reflections intensities were indexed, integrated and scaled using the autoproc
540 pipeline available at the beamline facility. OpSulf1 structure was solved using molecular
541 replacement with the AlphaFold2 predicted model as reference in PHASER (106). For
542 automatic model building we used BUCCANEER (107). Refinement was done in REFMAC5
543 (108) and COOT (109). Model and structure factors for OpSulf_1 were deposited in the Protein
544 Data Bank (PDB) with accession 9FVT. Corresponding data-processing and refinement
545 statistics are summarized in Table S4. The structural comparison of OpSulf with homologs
546 were performed using the PyMOL v.2.3.2 (Schrödinger, New York, NY, USA). For enzymes
547 that did not crystallize we used models generated with AlphaFold2 for structural analyzes (50).

548

549 **Liquid chromatography-mass spectrometry of mannose-sulfate and mannan digests**

550 Standards and digests were diluted in 90% UHPLC-grade and 10% (v/v) MilliQ water (Merck)
551 for LC-MS measurements. 5 µL were injected to an Accucore-150-amide HILIC column
552 (Thermo Fisher Scientific) held at 60 °C on a Thermo Fisher Vanquish Horizon UHPLC
553 coupled to a Thermo Fisher Q-Exactive Plus MS. Mobile phases A and B consisted of 10 mM
554 ammonium formate at pH 5 and UHPLC-grade acetonitrile, respectively. A gradient started
555 after 1 min at 90% B and decreased from 90% to 40% B over 40 min at a flow rate of 0.4 mL
556 min^{-1}. The column was equilibrated at 90% for 16 min at the end of each run. Mono- and
557 oligosaccharides was detected in negative mode. The detailed MS conditions are provided in
558 the SI material.

559 **Bacteria cultivation**

560 Growth experiments with *Polaribacter* spp. Hel1_33_49/78/96 and Hel1_88 were carried out
561 in HaHa-medium supplemented with 0.1 mg mL^{-1} yeast extract and 2 mg mL^{-1} mannan from
562 either *C. weissflogii* or *C. affinis* (110). We used *Polaribacter* sp. Hel1_33_78 for in depth
563 physiological experiments. Cells were harvested by centrifugation, the pellets chemically lysed.

564 Lysed cells, enzymes were activity tested on *C. weissflogii* and *C. affinis* mannan. Digests
565 occurred overnight using 3.5% Sea Salts (Sigma), 10 mM MOPS pH 7.5 and 0.5 mg mL^{-1}
566 mannan and were analyzed using carbohydrate-polyacrylamide gel electrophoresis (C-
567 PAGE). C-PAGE analysis was carried out as described in (111) with modifications described
568 in the SI. *Polaribacter* sp. Hel1_33_49 was grown in 3.5% Sea Salts (Sigma) with supplements
569 (110). The mannan was used as limiting carbon source at a concentration of 1 mg mL^{-1}. Growth
570 curves (absorbance 600 nm) were plotted with a logistic growth function using the non-linear
571 least squares method. Substrate consumption was verified qualitatively using C-PAGE.

572 **Enzyme assisted quantification of the mannan**

573 Cultures of *Conticribra weissflogii* were grown in NEPCC medium as described above.
574 Subsamples of 200 mL of the culture were filtered to remove cells and debris. The mannan in
575 the filtrate was purified using AEX. After desalting the mannan was digested PbSulf1-GHx and
576 PbGH92_1. Undigested sample served as negative control. Detection occurred with the
577 PAHBAH assay. Results were compared with a standard curve containing defined amounts of
578 mannan. The recovery was determined 80 ± 5% (n=3) by comparison to untreated mannan
579 **(fig S7C)**.

580 **Extraction of mannan from cellular, diatom biomass**

581 After diatom cultivation the cell pellet was freeze-dried and sequentially extracted using MilliQ
582 water (Merck), 0.4 M EDTA (pH 8) and 4 M NaOH with 0.1% NaBH4 (27). For 1 g of biomass
583 20 ml of sample were used. In each extraction step the sample was sonicated and centrifuged
584 at 14.000 x g for 10 minutes. NaOH extracts were neutralized to pH 7.5 using HCl and diluted
585 in MilliQ to < 500 mM NaCl. The mannan content in all extracts was determined as described
586 above.

587 **Biocatalytic detection of mannan in multiple diatom species**

588 The diatom strains *Thalassiosira pseudonana*, *Chaetoceros affinis* and *Thalassiosira rotula*
589 were cultivated as described above. 20 L of culture supernatant were concentrated after

590 filtration using GF/F. The filtrate was concentrated by ultrafiltration and then dialyzed to remove
591 salts. The dialyzed concentrate was purified by anionic exchange chromatography. The
592 purified mannan was again dialyzed and then lyophilized. The dialyzed and freeze-dried
593 samples were used as substrates for enzymatic assays using PbSulf1-GHx_1 and PbGH92_1.
594 Digested samples were analyzed with FACE (116).

595 **Nuclear magnetic resonance and chemical synthesis of oligosaccharides**

596 All chemicals used were reagent grade and used as supplied unless otherwise noted. A
597 detailed description of the structural elucidation and glycan synthesis processes is provided in
598 the supplementary information. The automated syntheses were performed on a custom-built
599 synthesizer (Potsdam-Golm, Germany)(112-115). More synthesis and analysis details are
600 provided in the SI.

601

602 **Acknowledgements:**

603 We thank Manual Liebeke for access to LC-MS devices and advise. We also thank C. Eschen,
604 P. Subramanya, P. Schoppmeier for large-scale cultivation of *Conticribra weissflogii* and
605 K. Imhoff for advice and support during sulfate quantification and T. Trautmann, A. Bolte and
606 K. Föll for technical support. We thank Hagen Buck-Wiese for help with the LC-MS analysis,
607 S. Niggemeier for assistance in cloning and expression and A. Sichert for help with genome
608 assembly. We thank André Scheffel for providing the *C. weissflogii* culture. We further thank
609 M. Schultz-Johansen for valuable discussions and his substantial help with the sampling
610 campaigns.

611 **Funding:** J-H.H. was funded by the German Research Foundation through the Heisenberg
612 program Grant (HE 7217/5-1). The work was supported by the European Research Council,
613 ERC grant, C-Quest, (Grant 101044738) to J-H.H. The work was supported by the PriME
614 collaboration of the Simons Foundation, Grant 970824 to J-H.H. This study was supported by
615 the German Federal Ministry of Education and Research (BMBF) in the frame of the BaMS-
616 BALI project (031B0915D1/2) and the German Research Foundation (DFG) for the Research
617 Unit FOR 2406 “Proteogenomics of Marine Polysaccharide Utilization” (POMPU) by Grants to
618 J-H.H. (HE 7217/2-3), T.S. (SCHW 595/10-3) and H.T (TE 813/2-3). The work was supported
619 by the Cluster of Excellence initiative (EXC-2077–390741603). C.J.C. was funded by MSCA
620 grant: MARINEGLYCAN (101029842). The Max-Planck Society supported P.H.S., J-H.H,
621 C.J.C. and R.K.S.

622 **Author contributions:** J.K. and J-H.H. planned and analyzed the experiments with support
623 by T.S.. J.K. and J-H.H. designed the artwork with help of M.B.. J.K. cloned and expressed the
624 genes, conducted all activity assays, purified the glycans and cultured marine diatoms. P.H.S.,
625 C.J.C. and R.K.S. synthesized the oligosaccharide and mannose-sulfate standards and
626 conducted all NMR experiments. V.S. provided structural models and refined the crystal
627 structure. H.T., C.S., J.K. and J-H.H. analyzed the metagenomes. L.R. purified the proteins,
628 set up crystallization experiments and edited the manuscript. M.B. conducted LC-MS

experiments. J-H.H. and J.K. wrote the manuscript with input from all authors. **Competing interests**: All authors declare that they have no competing interests. **Data and materials availability:** All data are available in the manuscript or the supplementary materials.

List of Supplementary Materials:

Supplementary Text

Figs. S1 to S31

Scheme S1

Table S1 to S6

Data S1 Chemical Synthesis

References and Notes

1. M. D. Purugganan, What is domestication? *Trends in Ecology & Evolution* **37**, 663-671 (2022).
2. M. A. Zeder, Core questions in domestication research. *Proceedings of the National Academy of Sciences* **112**, 3191-3198 (2015).
3. K. M. Olsen, J. F. Wendel, A Bountiful Harvest: Genomic Insights into Crop Domestication Phenotypes. *Annual Review of Plant Biology* **64**, 47-70 (2013).
4. E. V. Armbrust, The life of diatoms in the world's oceans. *Nature* **459**, 185-192 (2009).
5. J. R. Seymour, S. A. Amin, J.-B. Raina, R. Stocker, Zooming in on the phycosphere: the ecological interface for phytoplankton–bacteria relationships. *Nature Microbiology* **2**, 17065 (2017).
6. F. Unfried *et al.*, Adaptive mechanisms that provide competitive advantages to marine bacteroidetes during microalgal blooms. *The ISME Journal* **12**, 2894-2906 (2018).
7. S. Becker, J.-H. Hehemann, Laminarin Quantification in Microalgae with Enzymes from Marine Microbes. *Bio-protocol* **8**, e2666 (2018).
8. N. Barak-Gavish *et al.*, Bacterial lifestyle switch in response to algal metabolites. *Elife* **12** (2023).
9. M. R. Seyedsayamdost, R. J. Case, R. Kolter, J. Clardy, The Jekyll-and-Hyde chemistry of Phaeobacter gallaeciensis. *Nature Chemistry* **3**, 331-335 (2011).
10. E. E. Clerc *et al.*, Strong chemotaxis by marine bacteria towards polysaccharides is enhanced by the abundant organosulfur compound DMSP. *Nature Communications* **14**, 8080 (2023).
11. M. T. Croft, A. D. Lawrence, E. Raux-Deery, M. J. Warren, A. G. Smith, Algae acquire vitamin B12 through a symbiotic relationship with bacteria. *Nature* **438**, 90-93 (2005).
12. M. Uchimiya, W. Schroer, M. Olofsson, A. S. Edison, M. A. Moran, Diel investments in metabolite production and consumption in a model microbial system. *The ISME Journal* **16**, 1306-1317 (2022).
13. D. Muratore *et al.*, Complex marine microbial communities partition metabolism of scarce resources over the diel cycle. *Nature Ecology & Evolution* **6**, 218-229 (2022).
14. W. Petroski, D. M. Minich, Is There Such a Thing as "Anti-Nutrients"? A Narrative Review of Perceived Problematic Plant Compounds. *Nutrients* **12** (2020).
15. Y. Idota *et al.*, Relationship between Physical Parameters of Various Metal Ions and Binding Affinity for Alginate. *Biological and Pharmaceutical Bulletin* **39**, 1893-1896 (2016).
16. J. Li *et al.*, Microbial iron limitation in the ocean's twilight zone. *Nature* **633**, 823-827 (2024).
17. J.-H. Hehemann *et al.*, Adaptive radiation by waves of gene transfer leads to fine-scale resource partitioning in marine microbes. *Nature Communications* **7**, 12860 (2016).
18. C. B. Field, M. J. Behrenfeld, J. T. Randerson, P. Falkowski, Primary Production of the Biosphere: Integrating Terrestrial and Oceanic Components. *Science* **281**, 237 (1998).
19. M. F. White, C. R. Kahn, Insulin action at a molecular level – 100 years of progress. *Molecular Metabolism* **52**, 101304 (2021).
20. J. Monod, From Enzymatic Adaptation to Allosteric Transitions. *Science* **154**, 475-483 (1966).
21. A. Y. Valiakhmetov, A. V. Kuchin, N. E. Suzina, A. N. Zvonarev, A. O. Shepelyakovskaya, Glucose causes primary necrosis in exponentially grown yeast Saccharomyces cerevisiae. *FEMS Yeast Research* **19**, foz019 (2019).
22. G. S. Adams, B. A. Converse, A. H. Hales, L. E. Klotz, People systematically overlook subtractive changes. *Nature* **592**, 258-261 (2021).
23. A. Reichstein, Batman — An American Mr. Hyde? *Amerikastudien / American Studies* **43**, 329-350 (1998).
24. X. Jiang, Chinese Dialectical Thinking—the Yin Yang Model. *Philosophy Compass* **8**, 438-446 (2013).

25. S. Myklestad, O. Holm-Hansen, K. M. Vårum, B. E. Volcani, Rate of release of extracellular amino acids and carbohydrates from the marine diatom Chaetoceros affinis. *Journal of Plankton Research* **11**, 763-773 (1989).
26. L. I. Aluwihare, D. J. Repeta, A comparison of the chemical characteristics of oceanic DOM and extracellular DOM produced by marine algae. *Marine Ecology Progress Series* **186**, 105-117 (1999).
27. S. Vidal-Melgosa *et al.*, Diatom fucan polysaccharide precipitates carbon during algal blooms. *Nat Commun* **12**, 1150 (2021).
28. F. Vincent, C. Bowler, Diatoms Are Selective Segregators in Global Ocean Planktonic Communities. *mSystems* **5**, 10.1128/msystems.00444-00419 (2020).
29. H. Teeling *et al.*, Recurring patterns in bacterioplankton dynamics during coastal spring algae blooms. *Elife* **5**, e11888 (2016).
30. D. M. Needham, J. A. Fuhrman, Pronounced daily succession of phytoplankton, archaea and bacteria following a spring bloom. *Nature Microbiology* **1**, 16005 (2016).
31. W.-C. Chin, M. V. Orellana, P. Verdugo, Spontaneous assembly of marine dissolved organic matter into polymer gels. *Nature* **391**, 568-572 (1998).
32. A. Engel, S. Thoms, U. Riebesell, E. Rochelle-Newall, I. Zondervan, Polysaccharide aggregation as a potential sink of marine dissolved organic carbon. *Nature* **428**, 929-932 (2004).
33. J. Uitz, H. Claustre, B. Gentili, D. Stramski, Phytoplankton class-specific primary production in the world's oceans: Seasonal and interannual variability from satellite observations. *Global Biogeochemical Cycles* **24** (2010).
34. S. Malviya *et al.*, Insights into global diatom distribution and diversity in the world's ocean. *Proceedings of the National Academy of Sciences* **113**, E1516-E1525 (2016).
35. J. T. Staley, J. J. Gosink, Poles apart: biodiversity and biogeography of sea ice bacteria. *Annu Rev Microbiol* **53**, 189-215 (1999).
36. B. Avcı, K. Krüger, B. M. Fuchs, H. Teeling, R. I. Amann, Polysaccharide niche partitioning of distinct Polaribacter clades during North Sea spring algal blooms. *The ISME Journal* **14**, 1369-1383 (2020).
37. L. Kappelmann *et al.*, Polysaccharide utilization loci of North Sea Flavobacteriia as basis for using SusC/D-protein expression for predicting major phytoplankton glycans. *ISME J* **13**, 76-91 (2019).
38. C. Sidhu *et al.*, Dissolved storage glycans shaped the community composition of abundant bacterioplankton clades during a North Sea spring phytoplankton bloom. *Microbiome* **11**, 77 (2023).
39. F.-Q. Wang *et al.*, Particle-attached bacteria act as gatekeepers in the decomposition of complex phytoplankton polysaccharides. *Microbiome* **12** (2024).
40. T. B. Francis *et al.*, Changing expression patterns of TonB-dependent transporters suggest shifts in polysaccharide consumption over the course of a spring phytoplankton bloom. *The ISME Journal* **15**, 2336-2350 (2021).
41. J. Hevia-Orube *et al.*, Molecular and morphological analyses of solitary forms of brackish Thalassiosiroid diatoms (Coscinodiscophyceae), with emphasis on their phenotypic plasticity. *European Journal of Phycology* **51**, 11-30 (2016).
42. C. Ford, E. Percival, 1299. Carbohydrates of Phaeodactylum tricornutum. Part II. A sulphated glucuronomannan. *Journal of the Chemical Society (Resumed)*, 7042-7046 (1965).
43. T. Le Costaouëc, C. Unamunzaga, L. Mantecon, W. Helbert, New structural insights into the cell-wall polysaccharide of the diatom Phaeodactylum tricornutum. *Algal Research* **26**, 172-179 (2017).
44. B. Kloareg, Y. Badis, J. M. Cock, G. Michel, Role and Evolution of the Extracellular Matrix in the Acquisition of Complex Multicellularity in Eukaryotes: A Macroalgal Perspective. http://dx.doi.org/10.3390/genes12071059.
45. K. Le Mai Hoang *et al.*, Traceless Photolabile Linker Expedites the Chemical Synthesis of Complex Oligosaccharides by Automated Glycan Assembly. *Journal of the American Chemical Society* **141**, 9079-9086 (2019).

46. R. L. Hahnke *et al.*, Dilution cultivation of marine heterotrophic bacteria abundant after a spring phytoplankton bloom in the North Sea. *Environmental Microbiology* **17**, 3515-3526 (2015).
47. M. Richter, R. Rosselló-Móra, F. Oliver Glöckner, J. Peplies, JSpeciesWS: a web server for prokaryotic species circumscription based on pairwise genome comparison. *Bioinformatics* **32**, 929-931 (2016).
48. Y. K. Kwon *et al.*, Ochrovirga pacifica gen. nov., sp. nov., a novel agar-lytic marine bacterium of the family Flavobacteriaceae isolated from a seaweed. *Curr Microbiol* **69**, 445-450 (2014).
49. C. S. Robb, A. A. Mystkowska, J. H. Hehemann, Crystal structure of a marine glycoside hydrolase family 99-related protein lacking catalytic machinery. *Protein Sci* **26**, 2445-2450 (2017).
50. J. Jumper *et al.*, Highly accurate protein structure prediction with AlphaFold. *Nature* **596**, 583-589 (2021).
51. A. Varki *et al.*, Symbol Nomenclature for Graphical Representations of Glycans. *Glycobiology* **25**, 1323-1324 (2015).
52. T. Barbeyron *et al.*, Matching the Diversity of Sulfated Biomolecules: Creation of a Classification Database for Sulfatases Reflecting Their Substrate Specificity. *PLOS ONE* **11**, e0164846 (2016).
53. E. Drula *et al.*, The carbohydrate-active enzyme database: functions and literature. *Nucleic Acids Res* **50**, D571-D577 (2022).
54. G. Davies, B. Henrissat, Structures and mechanisms of glycosyl hydrolases. *Structure* **3**, 853-859 (1995).
55. A. G. Hettle *et al.*, The Molecular Basis of Polysaccharide Sulfatase Activity and a Nomenclature for Catalytic Subsites in this Class of Enzyme. *Structure* **26**, 747-758.e744 (2018).
56. Y. Zhu *et al.*, Mechanistic insights into a Ca2+-dependent family of alpha-mannosidases in a human gut symbiont. *Nat Chem Biol* **6**, 125-132 (2010).
57. F. Teufel *et al.*, SignalP 6.0 predicts all five types of signal peptides using protein language models. *Nature Biotechnology* **40**, 1023-1025 (2022).
58. A. Cartmell *et al.*, How members of the human gut microbiota overcome the sulfation problem posed by glycosaminoglycans. *Proceedings of the National Academy of Sciences* **114**, 7037-7042 (2017).
59. C. S. Robb *et al.*, Metabolism of a hybrid algal galactan by members of the human gut microbiome. *Nature Chemical Biology* **18**, 501-510 (2022).
60. K. T. Kim, L. E. Rioux, S. L. Turgeon, Alpha-amylase and alpha-glucosidase inhibition is differentially modulated by fucoidan obtained from Fucus vesiculosus and Ascophyllum nodosum. *Phytochemistry* **98**, 27-33 (2014).
61. C. Tara Oceans Consortium, P. Tara Oceans Expedition (2017) Registry of all samples from the Tara Oceans Expedition (2009-2013). (PANGAEA).
62. J.-H. Hehemann *et al.*, Biochemical and Structural Characterization of the Complex Agarolytic Enzyme System from the Marine Bacterium Zobellia galactanivorans*. *Journal of Biological Chemistry* **287**, 30571-30584 (2012).
63. G. Correc, J. H. Hehemann, M. Czjzek, W. Helbert, Structural analysis of the degradation products of porphyran digested by Zobellia galactanivorans beta-porphyranase A. *Carbohyd Polym* **83**, 277-283 (2011).
64. S. Becker, A. Scheffel, M. F. Polz, J. H. Hehemann, Accurate quantification of laminarin in marine organic matter with enzymes from marine microbes. *Appl Environ Microb* **83**, e03389 (2017).
65. F. Unfried *et al.*, Adaptive mechanisms that provide competitive advantages to marine bacteroidetes during microalgal blooms. *The ISME Journal* **12** (2018).
66. V. Smetacek, A. Zingone, Green and golden seaweed tides on the rise. *Nature* **504**, 84-88 (2013).
67. L. Reisky *et al.*, A marine bacterial enzymatic cascade degrades the algal polysaccharide ulvan. *Nat Chem Biol* **15**, 803-812 (2019).

68. O. I. Nedashkovskaya *et al.*, Formosa agariphila sp. nov., a budding bacterium of the family Flavobacteriaceae isolated from marine environments, and emended description of the genus Formosa. *Int J Syst Evol Microbiol* **56**, 161-167 (2006).
69. A. J. Mann *et al.*, The genome of the alga-associated marine flavobacterium Formosa agariphila KMM 3901T reveals a broad potential for degradation of algal polysaccharides. *Appl Environ Microbiol* **79**, 6813-6822 (2013).
70. E. V. Armbrust, The life of diatoms in the world's oceans. *Nature* **459**, 185-192 (2009).
71. C. de Vargas *et al.*, Eukaryotic plankton diversity in the sunlit ocean. *Science* **348**, 1261605 (2015).
72. C. d. Vargas *et al.* (2015) First Tara Oceans V9 rDNA metabarcoding dataset.
73. M. Bligh, N. Nguyen, H. Buck-Wiese, S. Vidal-Melgosa, J. H. Hehemann, Structures and functions of algal glycans shape their capacity to sequester carbon in the ocean. *Curr Opin Chem Biol* **71**, 102204 (2022).
74. C. S. Hassler, V. Schoemann, C. M. Nichols, E. C. V. Butler, P. W. Boyd, Saccharides enhance iron bioavailability to Southern Ocean phytoplankton. *Proceedings of the National Academy of Sciences* **108**, 1076-1081 (2011).
75. F. X. Ferrer-González *et al.*, Resource partitioning of phytoplankton metabolites that support bacterial heterotrophy. *The ISME Journal* **15**, 762-773 (2021).
76. S. Becker *et al.*, Laminarin is a major molecule in the marine carbon cycle. *Proc Natl Acad Sci U S A* **117**, 6599-6607 (2020).
77. J. Kurreck, J. W. Engels, F. Lottspeich, *Bioanalytik* (Springer Spektrum Berlin, Heidelberg, 2021), vol. 4.
78. H. M. Berman *et al.*, The Protein Data Bank. *Nucleic Acids Res* **28**, 235-242 (2000).
79. K. M. Wheeler *et al.*, Mucin glycans attenuate the virulence of Pseudomonas aeruginosa in infection. *Nature Microbiology* **4**, 2146-2154 (2019).
80. C. Cisternas-Novoa, C. Lee, A. Engel, Transparent exopolymer particles (TEP) and Coomassie stainable particles (CSP): Differences between their origin and vertical distributions in the ocean. *Marine Chemistry* **175**, 56-71 (2015).
81. E. A. Pelve, K. M. Fontanez, E. F. DeLong, Bacterial Succession on Sinking Particles in the Ocean's Interior. *Frontiers in Microbiology* **8** (2017).
82. S. Thiele, M. Fuchs Bernhard, R. Amann, H. Iversen Morten, Colonization in the Photic Zone and Subsequent Changes during Sinking Determine Bacterial Community Composition in Marine Snow. *Appl Environ Microb* **81**, 1463-1471 (2015).
83. H. Teeling *et al.*, Substrate-Controlled Succession of Marine Bacterioplankton Populations Induced by a Phytoplankton Bloom. *Science* **336**, 608-611 (2012).
84. D. M. Needham *et al.*, Dynamics and interactions of highly resolved marine plankton via automated high-frequency sampling. *The ISME Journal* **12**, 2417-2432 (2018).
85. S. J. Giovannoni, SAR11 Bacteria: The Most Abundant Plankton in the Oceans. *Annual Review of Marine Science* **9**, 231-255 (2017).
86. A. Dadon-Pilosof *et al.*, Surface properties of SAR11 bacteria facilitate grazing avoidance. *Nature Microbiology* **2**, 1608-1615 (2017).
87. J. Sun *et al.*, One carbon metabolism in SAR11 pelagic marine bacteria. *PLoS One* **6**, e23973 (2011).
88. B. J. Shapiro *et al.*, Population genomics of early events in the ecological differentiation of bacteria. *Science* **336**, 48-51 (2012).
89. A. S. Utada *et al.*, Vibrio cholerae use pili and flagella synergistically to effect motility switching and conditional surface attachment. *Nature Communications* **5**, 4913 (2014).
90. Y. Yawata *et al.*, Competition-dispersal tradeoff ecologically differentiates recently speciated marine bacterioplankton populations. *Proc Natl Acad Sci U S A* **111**, 5622-5627 (2014).
91. K. Moor *et al.*, High-avidity IgA protects the intestine by enchaining growing bacteria. *Nature* **544**, 498-502 (2017).
92. J. M. Grondin, K. Tamura, G. Dejean, D. W. Abbott, H. Brumer, Polysaccharide utilization loci: fueling microbial communities. *J Bacteriol* **199**, e00860-00816 (2017).
93. N. M. Koropatkin, E. A. Cameron, E. C. Martens, How glycan metabolism shapes the human gut microbiota. *Nature Reviews Microbiology* **10**, 323-335 (2012).

94. R. B. Cassie *et al.*, Carbohydrate-active enzymes from Akkermansia muciniphila breakdown mucin O-glycans to completion. *bioRxiv* 10.1101/2024.03.27.586211, 2024.2003.2027.586211 (2024).
95. O. Gainza, J. Romero, Effect of mannan oligosaccharides on the microbiota and productivity parameters of Litopenaeus vannamei shrimp under intensive cultivation in Ecuador. *Scientific Reports* **10**, 2719 (2020).
96. A. M. Martin-Platero *et al.*, High resolution time series reveals cohesive but short-lived communities in coastal plankton. *Nature Communications* **9**, 266 (2018).
97. G. Reintjes *et al.*, Short-term changes in polysaccharide utilization mechanisms of marine bacterioplankton during a spring phytoplankton bloom. *Environmental Microbiology* **22**, 1884-1900 (2020).
98. B. Langmead, S. L. Salzberg, Fast gapped-read alignment with Bowtie 2. *Nature Methods* **9**, 357-359 (2012).
99. P. J. Harrison, R. E. Waters, F. J. R. Taylor, A BROAD SPECTRUM ARTIFICIAL SEA WATER MEDIUM FOR COASTAL AND OPEN OCEAN PHYTOPLANKTON1. *Journal of Phycology* **16**, 28-35 (1980).
100. A. Engel, N. Händel, A novel protocol for determining the concentration and composition of sugars in particulate and in high molecular weight dissolved organic matter (HMW-DOM) in seawater. *Marine Chemistry* **127**, 180-191 (2011).
101. P. J. Shilling *et al.*, Improved designs for pET expression plasmids increase protein production yield in Escherichia coli. *Communications Biology* **3**, 214 (2020).
102. J. J. Almagro Armenteros *et al.*, SignalP 5.0 improves signal peptide predictions using deep neural networks. *Nature Biotechnology* **37**, 420-423 (2019).
103. I. S. Carrico, B. L. Carlson, C. R. Bertozzi, Introducing genetically encoded aldehydes into proteins. *Nat Chem Biol* **3**, 321-322 (2007).
104. V. Solanki *et al.*, Glycoside hydrolase from the GH76 family indicates that marine Salegentibacter sp. Hel_I_6 consumes alpha-mannan from fungi. *ISME J* **16**, 1818-1830 (2022).
105. J. H. Hehemann *et al.*, Transfer of carbohydrate-active enzymes from marine bacteria to Japanese gut microbiota. *Nature* **464**, 908-912 (2010).
106. A. J. McCoy *et al.*, Phaser crystallographic software. *J Appl Crystallogr* **40**, 658-674 (2007).
107. K. Cowtan, The Buccaneer software for automated model building. 1. Tracing protein chains. *Acta Crystallogr D Biol Crystallogr* **62**, 1002-1011 (2006).
108. G. N. Murshudov *et al.*, REFMAC5 for the refinement of macromolecular crystal structures. *Acta Crystallogr D Biol Crystallogr* **67**, 355-367 (2011).
109. P. Emsley, B. Lohkamp, W. G. Scott, K. Cowtan, Features and development of Coot. *Acta Crystallogr D Biol Crystallogr* **66**, 486-501 (2010).
110. R. L. Hahnke, J. Harder, Phylogenetic diversity of Flavobacteria isolated from the North Sea on solid media. *Syst Appl Microbiol* **36**, 497-504 (2013).
111. M. Robb, J. K. Hobbs, A. B. Boraston, Separation and Visualization of Glycans by Fluorophore-Assisted Carbohydrate Electrophoresis. *Methods Mol Biol* **1588**, 215-221 (2017).
112. C. J. Crawford *et al.*, Automated Synthesis of Algal Fucoidan Oligosaccharides. *Journal of the American Chemical Society* **146**, 18320-18330 (2024).
113. C. Crawford, S. Oscarson, Optimized Conditions for the Palladium-Catalyzed Hydrogenolysis of Benzyl and Naphthylmethyl Ethers: Preventing Saturation of Aromatic Protecting Groups. *European Journal of Organic Chemistry* **2020**, 3332-3337 (2020).
114. O. J. Plante, E. R. Palmacci, P. H. Seeberger, Automated Solid-Phase Synthesis of Oligosaccharides. *Science* **291**, 1523-1527 (2001).
115. O. J. Plante, R. B. Andrade, P. H. Seeberger, Synthesis and Use of Glycosyl Phosphates as Glycosyl Donors. *Organic Letters* **1**, 211-214 (1999).